Versão do arquivo anexado / Version of attached file:

Versão do Editor / Published Version

Mais informações no site da editora / Further information on publisher's website:

https://www.scielo.br/scielo.php?script=sci_arttext&pid=S1516-14392018000600229

DOI: 10.1590/1980-5373-MR-2018-0059

Direitos autorais / Publisher's copyright statement:

Influence of clay surfactants polarity on the crystallization and rheological behavior of nanocomposites of PDLLA

Renata Brandão Brito Ramos[a], Patrícia Moraes Sinohara Souza[a] , Ana Rita Morales[a]*

[a] Departamento de Engenharia de Materiais e de Bioprocessos, Faculdade de Engenharia Química, Universidade Estadual de Campinas (UNICAMP), Campinas, SP, Brasil

The effect of clay hydrophobicity on the cold crystallization and rheological properties of nanocomposites of poly(D,L-lactic acid) (PDLLA) was investigated. Crystallization was evaluated by DSC for isothermal and non-isothermal conditions. The clay modified with a hydrophilic surfactant acts as a nucleating agent, while the clay modified with a hydrophobic surfactant acts in an opposite way. The Avrami and Ozawa parameters showed a three-dimensional spherulitic growth for all samples and the activation energy increased for the hydrophobic clay and decrease for the hydrophilic one. The equilibrium melting point for the PDLLA was found at 161ºC, being slightly altered as function of the surfactant polarity. The rheological behavior was investigated in terms of Isothermal Flow-Induced Crystallization and Structural Recovery. The hydrophobic clay showed to reduce the mobility of chains and retard the chain relaxation, which is attributed to the formation of a network, while the hydrophilic clay increased the chain mobility.

Keywords: *PDLLA, nanocomposites, organoclays, crystallization.*

1. Introduction

Poly(lactic acid) (PLA) is a biodegradable polymer, which has many important characteristics like good mechanical properties when compared to commercial polymers such as polystyrene and polyethylene terephthalate. It is produced from 100% of renewable resources such as corn, potato, sugar and others[1]. Furthermore, PLA has been a promising polymer for many applications such as drug delivery, food packing, tissue engineering, etc[2]. PLA-based materials are already produced at large scale, and the use of organoclays fillers could even promote its applications in packing by enhancement of gas barrier properties[3].

Although PLA possesses many desirable properties, its crystallization rate is extremely slow in comparison with commercial thermoplastics. The most viable method to increase the overall crystallization of polymers is the addition of a nucleating agent. Clay was used by Okamoto and coworkers[4], who found that the overall crystallization rate and spherulitic texture of PLA were strongly influenced by montmorillonite particles. At the same time, they found that blending of low-molecular weight aliphatic acid also increased the crystallization rate[5]. Thus, a key point to improve properties is to understand the PLA crystallization process in order to control its thermal and mechanical resistance, degradation rate, optical and barrier properties[6].

Depending on the process conditions, PLA can crystallize in α, β, or γ forms. The different crystalline morphologies could affect the material properties[7]. It is known that the crystallization temperature (T_c) is directly related to the

thermodynamic and kinetic of structure formation. Moreover, different morphologies can be obtained altering the degree of undercooling for the crystallization of the flexible chain polymers from the melting[8]. Besides the processing conditions, the incorporation of inorganic fillers in polymers can improve or hinder the crystallization.

According to Krikorian et al.[8] the addition of compatible filler in matrix polymer results in an increased spherulite growth rate. In their other study with nanofillers, the interaction between the silicate layers and the PLA chains during the crystallization was studied. In pure poly(L,L-lactic acid) (PLLA) the inter-chain interactions occurs before helix formation. Crystallization of PLLA, from the melt or from solution, results in α form, with helical chain conformation where two chains are interacting in an orthorhombic unit cell. In the presence of an exfoliated morphology of a silicate, the helix formation starts earlier and the silicate layers hinders the inter-chain interactions necessary for crystal nucleation. On the other hand, if the silicate presents an intercalated morphology inter and intra-chain interactions are simultaneous leading to faster crystallization[9].

The isothermal cold crystallization kinetics of PLA with nucleating agents ($CaCO_3$, TiO_2, and $BaSO_4$, content from 0.5 to 2.0 wt%) was also investigated. The findings showed that, even by blending with nucleating agents, PLA had a maximum crystallinity of 14.9%[10].

Although much work has been done to investigate the effect of nucleating agent on the crystallization of PLLA, less work has been done to investigate the effects of nucleating agent on PDLLA crystallization[11,12]. Fukushima et al.[13] reported the thermal characterization of poly (D-lactic acid) (PDLA)

nanocomposite. They found a considerable thermo-mechanical improvement of the PDLA matrix by the incorporation of Cloisite 30B. Furthermore, they found that the incorporation of the clay considerably favors kinetics and extent of crystallization of the PDLA on heating[13].

There are some studies about the effect of organoclays in biodegradable properties. Souza et al.[14] studied nanocomposites of PDLLA with organoclays Cloisite 20A and Cloisite 30B prepared by melt intercalation, which presented an intercalated/exfoliated structure. In the evaluation of hydrolytic degradation they noted that the presence of organoclays can decrease the rate of degradation possibly due to the barrier effect of clay layers and/or the higher degree of crystallinity in the nanocomposite samples.

Wokadala et al.[15] studied the influence of nanoclay hydrophobicity on the crystallization kinetics. They found that hydrophobic clays hindered the crystallization of the PLA due to decreased mobility of the amorphous phase[15].

The objective of this work is to investigate the effect of the clay hydrophobicity on the cold crystallization kinetics and its correlation with rheological behavior of a commercial PDLLA and its nanocomposites. The activation energies for non-isothermal crystallization and the equilibrium melting point have also been evaluated. Furthermore, shear induced crystallization and structural recovery tests were found to be very effective to elucidate the observed crystallization results.

2. Experimental

2. 1 Materials

Poly(D,L-lactic acid) (PDLLA) Ingeo 4042D from Natureworks with content of D-lactic acid of $4.25 \pm 0.55\%$ was used to prepare the nanocomposites. Two types of organically modified montmorillonite (MMT), Cloisite 30B® and Cloisite20A® from Southern Clay Product Inc. were used as received. These organoclays are natural montmorillonite clays modified with different quaternary ammonium salts. The specifications of clays are listed in Table 1 according to the data provided by the supplier.

2.2 Preparation of clay/PDLLA nanocomposites

Nanocomposites were prepared with Cloisite 30B (PDLLA30B) and Cloisite20A (PDLLA20A), with clay content of 5% (w/w), using the melting intercalation technique. Initially, the PDLLA pellets and the organoclays were dried at 80°C for 4 hours. The components were processed in a mixer *Drais* MH type, MH100 model where the premixed components were mixed by very high shear until the melting. Although this system does not have a time and temperature control, it is able to apply a very good mixing condition for thermoplastics materials. The samples were obtained with a thickness of around 0.5 mm in a press MH, Q/FMot8ton model, molded at 210°C. The procedure was also conducted

for the PDLLA pellets without clay. The samples are the same from previous studies on biodegradation end ecotoxicity realized by Souza et al.[14,17].

2.3 Differential scanning calorimetry

Isothermal and non-isothermal crystallization studies were performed on a Mettler Toledo differential scanning calorimeter (DSC), Star model, under a constant nitrogen flow of 50mLmin[(-1)]. Samples of 5-10 mg were weighed accurately and encapsulated in perforated aluminum pans. Standard indium was employed for the temperature and heat flow calibration.

The crystallization was assessed during the heating (cold crystallization), because all samples did not showed any exothermic event in the cooling.

Figure 1 shows the thermal processes at DSC. For the isothermal experiments (Figure1 (a)), the samples were heated at a rate of 100°Cmin[-1] from room temperature to 200°C (Process I), held at that same temperature for 5 minutes (Process II), and then cooled at a rate of -10°Cmin[-1] to room temperature (Process III). After this, the sample was heated at a rate of 100 °C min^{-1} to the isothermal temperature (105; 110; 115 and 120°C) (Process IV) and kept at this temperature during 30 minutes (Process V). After this period, the temperature was ramped to 200°C at a heating rate of 10°Cmin[-1] to probe the melting point in the isotherm crystallization temperature and determine the equilibrium melting point (Process VI).

For the non-isothermal experiments (Figure 1 (b)), the samples were heated at a specific rate (0.5; 1.0; 1.5; 2.5 and 5.0 °C.min^{-1}) from 0°C to 200°C (Stage I), held at that same temperature for 5 minutes (Stage II), and then cooled at a specific rate to 0°C (Stage III). After this, the sample was heated again at a specific rate from 0°C to 200°C (Stage IV).The crystallinity and thermal properties was evaluated by the non-isothermal crystallization method, described in the Figure 1 (b).

Degree of crystallinity for molded samples was calculated from the first heating data according to the Equation (1), which the cold crystallization enthalpy was discounted from the total melting enthalpy. Furthermore, the degree of crystallinity from the second heating data was also calculated.

$$X_c(\%) = \frac{(\Delta H_m - \Delta H_c)}{\Delta H_m^\infty} \times 100 \qquad (1)$$

Where ΔH_m and ΔH_c are the melting and the cold crystallization enthalpies, respectively, and ΔH_m^∞ is the reference $\Delta H_m = 93.6$ J g^{-1} for PLA crystals[18].

2.4 Rheological properties

The dynamic rheological properties were analyzed in a rheometer DHR-2 from TA Instruments, with geometry of parallel plates, plate's diameter of 25 mm and gap between plates of 1 mm, under nitrogen atmosphere, at 180 °C. The

Table 1. Specifications of organoclays Cloisite 20A® and Cloisite 30B®[16].

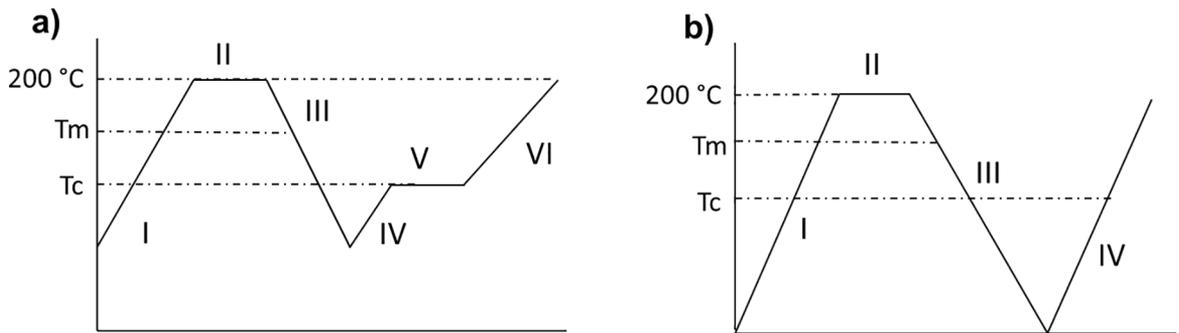| Characteristics	Cloisite 20A®	Cloisite 30B®
Organic modifier	$CH_3 - N^+ - HT$ with CH_3 and HT substituents Dialkyldimethylammonium	$CH_3 - N^+ - T$ with CH_2CH_2OH substituents Alkyl methyl di(2-hydroxyethyl) ammonium
% Moisture	< 2 %	< 2 %
% Weight Loss on Ignition	38 %	30 %
Particle size	10% less than 2 μm 50% less than 6 μm 90% less than 13 μm	10% less than 2 μm 50% less than 6 μm 90% less than 13 μm
Specific Gravity	1.77 g cm^{-3}	1.98 g cm^{-3}
DRX results	d(001) = 2.42 nm	d(001) = 1.85 nm

T= tallow (~65 % C18; ~30 % C16; ~5 % C14)

Figure 1. Temperature program for (a) isothermal crystallization kinetic and equilibrium melting point determination and (b) non-isothermal crystallization kinetic.

storage modulus G' (ω), loss modulus G" (ω) and complex viscosity (η*), where ω is the frequency, were measured.

2.5 Isothermal Flow-Induced Crystallization

Studies of the flow-induced crystallization were done using a rheometer DHR-2 from TA Instruments, with parallel-plates geometry (25 mm diameter) and gap of 1.0 mm. The procedure described by Farah and Bretas[19] was used. The material was melted at 180 and after 5 min at this latter temperature; the sample was quenched down to 110 °C. After temperature stabilization, a shear rate (γ) of 0.01 s^{-1} was imposed to the sample and the shear stress (τ) was monitored as a function of time (t). From these measurements, the t_{growth} was calculated; this time was defined as the time at which the shear stress increased abruptly.

2.6 Structural Recovery

Structural recovery experiments were conducted under nitrogen atmosphere according to the procedure described by Wang et al.[20] at low-amplitude oscillatory shear mode (ω= 1 rad/s, strain =1%) for the measuring of the initial storage modulus (G' (0)); the samples were submitted at a steady shear (γ = 2 s^{-1}) during 600 s and the linear storage

modulus (G' (t)) was recorded again under the same initial conditions. The G' at plateau (G'(equi)) was measured at the end of structural recovery. The behavior of PDLLA chain motion and relaxation associated to the structural disorientation was determined as the time from the cessation of shear to the equilibrium of structural recovery, t_{equi}.

3. Results and Discussion

3.1 Effects of organoclays in the crystallization behavior of PDLLA

Figure 2 shows the second heating curves for the PDLLA and nanocomposites at different scanning rates. The data obtained from these curves were listed in Table 2.

No changing was observed in Tg. The cold crystallization peak (T_{cc}) and the onset crystallization temperature (T_{conset}) were shifted to lower temperature, approximately 2°C, by the presence of organo clay Cloisite 30B. This is the first evidence that the Cloisite 30B accelerates the crystallization. Opposite behavior was observed to organoclay Cloisite 20A, in which the crystallization is retarded. Same behavior has
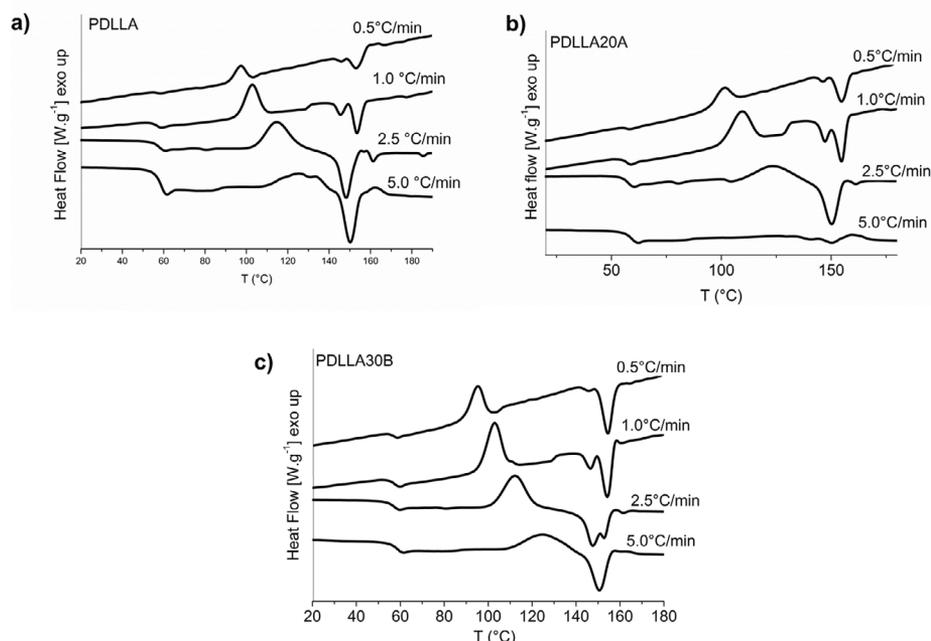
Figure 2. DSC scans with different heating rates (second heating): (a) PDLLA, (b) PDLLA20A, (c) PDLLA30B.

Table 2. Data obtained from the DSC second heating at scanning rate of 2.5°C min^{-1}.

Samples	T_g	$T_{c\ onset}$	T_{cc}	ΔH_{cc}	T_m	ΔH_m	X_c^1	X_c^2
	°C			J g^{-1}	°C	J g^{-1}	%	
PDLLA	57	105	115	26.9	148	28.3	0.4	30
PDLLA20A	57	113	123	15.0	151	18.5	0.2	21
PDLLA30B	56	102	112	33.0	148	29.3	1.8	33

[1]Degree of crystallinity of molded samples.

[2]Degree of crystallinity from the second heating scan.

been already observed for Cloisite 20A and unmodified sepiolite on crystallization of PLA nanocomposites[21].

X-Ray Difraction analysis of the samples used in this study were presented in a previous work[17]. The results of basal spacing for PDLLA20A and PDLLA30B were 3.15 nm e 3.32 nm, respectively. The basal spacing increasing of nanocomposites related to its pure organoclays was 0.46 for PDLLA20A and 1.46 nm for PDLLA30B. Transmission Electron Microscopy images of these samples were also presented in a previous work and it was noted a more homogeneous dispersion of clay in the sample with Cloisite 30B[14]. These findings were attributed to the greater chemical interaction presence of carbonyl groups of its organic modifier, which possibly favored strong interactions, of hydrogen with the carbonyl group of the polymer[22].

The crystallinity degree for the molded samples (X_c^1) was founded to be too low, although a little increase was observed for the Cloisite 30B nanocomposite. Considering the second run on the DSC the effects of the nanoclays can be observed. The Cloisite 20A caused a reduction on X_c^2 while the Cloisite 30 enhance it. Souza et al.[17] studied these same samples by DSC analysis and found crystallinity

degree for PDLLA as 3% and 6% for nanocomposites for heating/cooling rate of 10°C.min^{-1}. The lower results of X_c obtained in that study in relation to the present evaluation can be associated to the faster rate used that is not favorable to the formation of crystallites.

The PDLLA showed a double melting point, more pronounced at low heating rates. This behavior has been reported by many other studies and it was attributed to slow rates of crystallization and recrystallization, wherein the low temperature peak is related to the melting of some amount of the original crystals and the high temperature peak to the melting of crystals formed through a melt-recrystallization process during a heating scan[18,23]. The double melting peaks were attributed also to the formation of a double crystalline structure: β in coexistence with α or α' phases. The α' was described to be similar to α structure, but less ordered[24]. The PLA can present different crystal structures depending on the crystallization conditions. The α phase originates from the melt and solution with a orthorhombic cell with parameters a = 1.05 nm, b = 0.61 nm and c = 2.88 nm. The β phase can be originated by stretching of the α phase at high draw-ratio and high temperature. The γ phase was also

described for PLA as the more ordered caused by the crystal modification[25,26].

3.2 Isothermal Crystallization behavior

Isothermal experiments of PDLLA and nanocomposites obtained by heating the sample to the designated crystallization temperature are shown in Figure 3[27]. It was observed that the crystallization peak shifts to a higher value on time with increasing Tc. Furthermore, the crystallization of PDLLA is strongly affected by nanoclay addition. The shift is more pronounced for PDLLA30B than PDLLA and PDLLA20A. The addition of Cloisite 30B shortens the time to reach the crystallization halftime, indicating a faster crystallization rate, as shown in Table 3. This result suggests that during the isothermal crystallization, Cloisite 30B acts as a nucleating agent and contributes to an improvement in the crystallinity of PDLLA. Besides the nucleating effect, this result could be also intensified due to the degradation of PDLLA chains in this nanocomposite. Souza et al.[14] verified that the production of nanocomposites with Cloisite 30B presented a reduction of 44% in the weight average molecular weight (Mw) of the PDLLA. However, for the Cloisite 20A is the opposite, there was a decreased of the crystallization halftime.

The isothermal crystallization kinetics were studied by Avrami equation, which predicts the crystalline fraction, X(t), as a function of time at a constant temperature[28]. The relative crystallinity (X_t) versus a different crystallization time (t) was calculated according to the following Equation (2).

$$X_t = \int_0^t \frac{dH}{dt} dt \Big/ \int_0^\infty \frac{dH}{dt} dt \qquad (2)$$

Where dHc/dt is the rate of heat evolution. X_t, obtained from the area of the isothermal crystallization peak, in function of time is shown in Figure 3.

Isotherms in sigmoidal form are being shifted to high time values with increasing Tc, which means that the crystallization rate decreases. Figure 4 shows that only the PDLLA30B sample has the lowest initial nucleation time, which means that Cloisite 30B assists and accelerates the nucleation[27].

3.3 Avrami theory

The theory of Avrami was used to analyze the increase of the relative crystallinity (X_t) with time (t), according to the Equation (3).

$$X_t = 1 - \exp(Kt^n) \qquad (3)$$

The linearization of Equation 3 leads to a graph of log (-ln (1-Xt)) versus log (t), Figure 5, where X_t is the relative crystallinity at different times, t is the period of the crystallization process, K and n values denote the crystallization rate constant and the Avrami exponent, respectively. K is the growth rate constant, and n is related to the processes of nucleation and crystal growth. It is associated to the type of nucleation, crystal morphology and occurrence of secondary crystallization[28]. The crystallization rate K and the Avrami
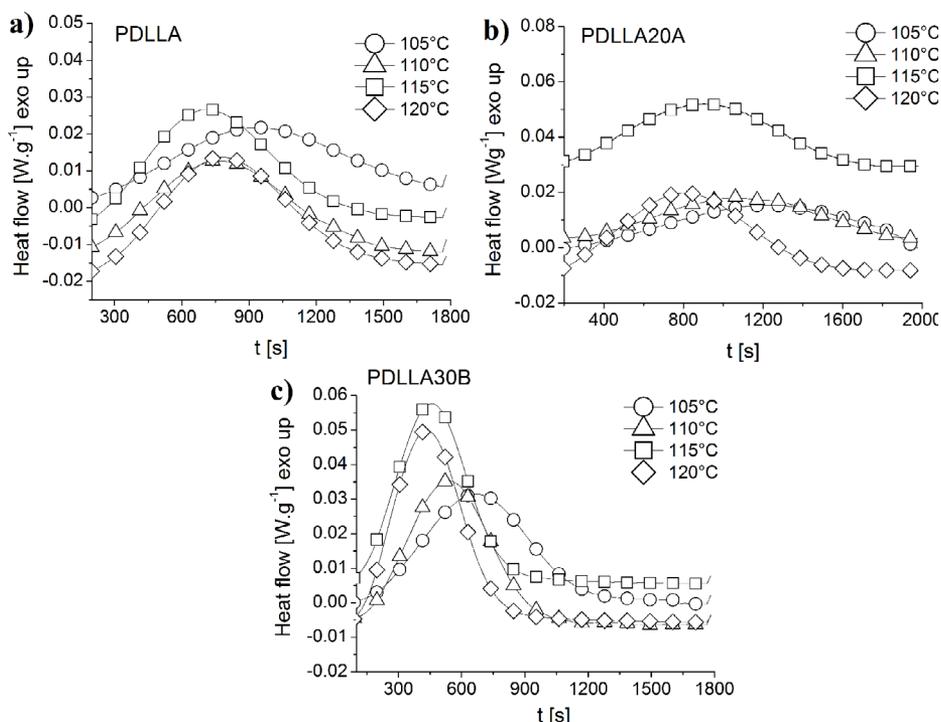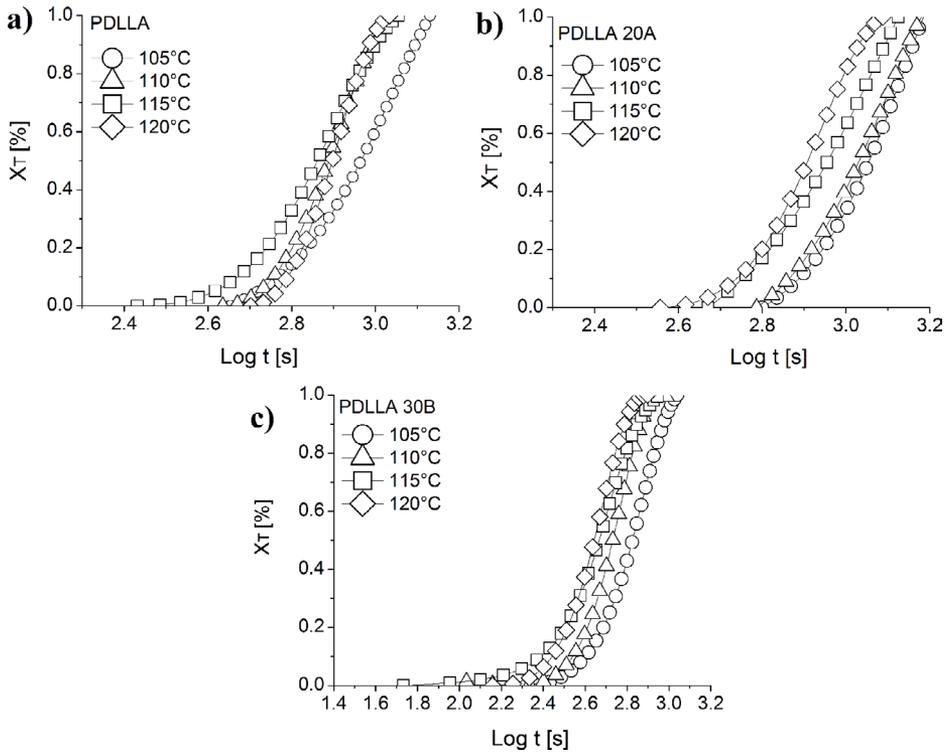

Figure 3. Isothermal crystallization in different temperatures: (a) PDLLA, (b) PDLLA20A, (c) PDLLA30B. Reproduced from Ref.[27], with permission of 13th Congresso Brasileiro de Polímeros - CBPol/Associação Brasileira de Polímeros - ABPol.

Table 3. Kinetics parameters of the PDLLA and the nanocomposites as function of crystallization temperature.

Samples	Tc	$t_{1/2}$	G 10^{-3}	$n_{average}$	Kaverage
	°C	s	s^{-1}		s^{-1}
PDLLA	105	924	1.08		
	110	761	1.31		
	115	717	1.39	3.8	3.4×10^{-12}
	120	814	1.23		
PDLLA20A	105	1173	0.85		
	110	1118	0.90		
	115	886	1.13	4.1	1.7×10^{-11}
	120	750	1.33		
PDLLA30B	105	665	1.50		
	110	501	2.00		
	115	486	2.06	3.6	1.6×10^{-09}
	120	421	2.37		

Figure 4. Relative crystallinity versus crystallization time: (a) PDLLA, (b) PDLLA20A, (c) PDLLA30B. Reproduced from Ref.[27], with permission of 13th Congresso Brasileiro de Polímeros - CBPol/Associação Brasileira de Polímeros - ABPol.

exponent n are obtained from the intercept and slope of the curves, respectively, and are reported in Table 3.

The bulk crystallization half-time ($t_{1/2}$), the time required to reach 50% of total crystallinity, was calculated as shown in Equation (4).

$$t_{1/2} = \left(\frac{\ln 2}{K} \right)^{1/n} \quad (4)$$

Commonly, $t_{1/2}$ is employed to characterize the crystallization rate directly. The longer the crystallization halftime, the slower the crystallization rate (G), as Equation (5).

$$G = \frac{1}{t_{1/2}} \quad (5)$$

The Avrami exponent n shown in Table 3 was in the range of 3.6 to 4.1 for the three samples. The higher n values are attributed to three-dimensional spherulitic growth with
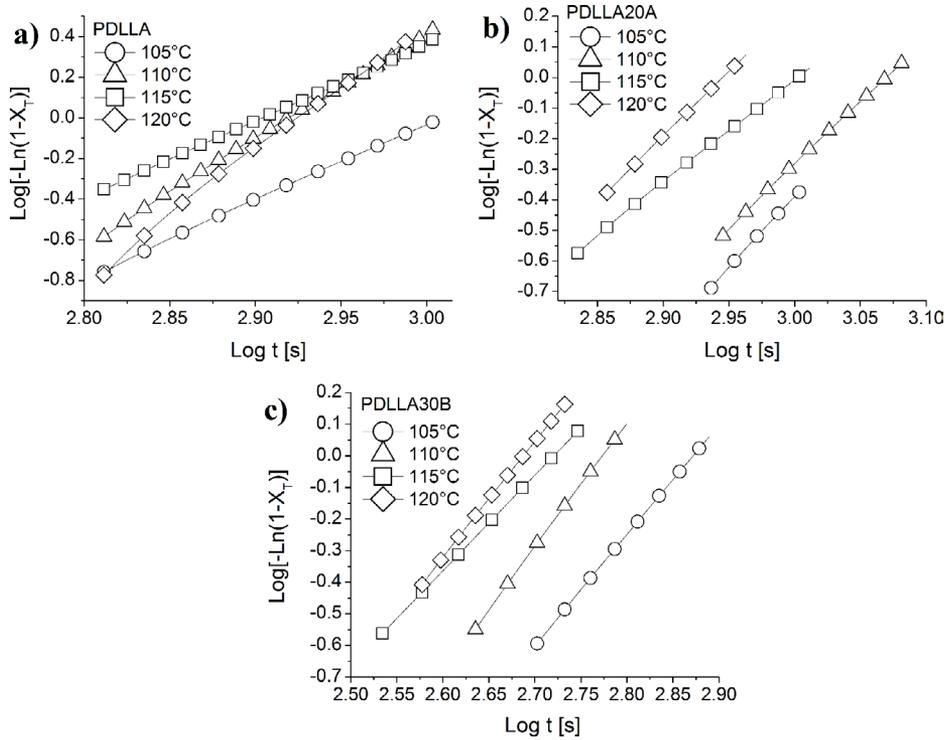
Figure 5. Plots of log[-ln(1-X_t)] versus log t for the isothermal crystallization at specific temperatures: (a) PDLLA, (b) PDLLA20A, (c) PDLLA30B.

a sporadic or a combination of sporadic and simultaneous nucleation type. Nonintegral of n values indicate a combination of thermal and athermal nucleation mechanisms[6].Furthermore, in the literature, there are different values reported, ranging from 2 to 5.4[2]. The values obtained in the study are acceptable because of the difference in values can be attributed to several factors such as the mechanism of nucleation, the form of the crystal growth, D-lactide content and the difference in the techniques used in determining of the results. Accordingly, it is inferred that the crystal growth has a spherical three-dimensional morphology with a combination of thermal and athermal nucleation in the PDLLA systems.

A good approach for n values higher than 3 was done by Lorenzo et al.[29]. The Avrami index n = n_d + n_n and can only result on integer numbers 1, 2 or 3, associated to the crystal dimensions and n_n represents the time dependence of the nucleation where the 0 would be for the instantaneous nucleation and 1 for sporadic nucleation. The PDLLA nucleation and crystal growing is a complex process since it presents a slow crystallization by cooling and a cold crystallization by heating, what means that the nucleation may be somewhat in between completely instantaneous or completely sporadic and that the supercooling induces to indices in between 3 and 4. Also, the n exponent cannot be taken as exact and straight information of the crystals morphology as its determination may be complicated by volume changes due to phase transformation, incomplete crystallization or different mechanisms involved during

the process causing it to n fractional values[29]. The Avrami's theory could be a precise solution only for well defined morphologies like line, circles or spheres. Although for more complex morphologies this theory can be applied for an approximated estimation for crystallization process[30].

As shown in Table 3, the K value had an increase of two orders of magnitude for the sample with Cloisite 30B. This means that the Cloisite 30B accelerates the crystallization process of the PDLLA. Furthermore, the bulk crystallization half-time in the case of PDLLA30B is significantly smaller than PDLLA and PDLLA20A, confirming that the nanoclay containing less hydrophobic surfactant assists in the crystallization. This phenomenon has been noted with additives having high interfacial energy when added to the polymer[8].In addition, the crystallization rate (G) for the sample PDLLA30B is almost twice of the sample PDLLA20A, showing that the hydrophobic surfactant hinder the crystallization process.

Wokadala et al.[15] have studied the influence of the nanoclay hydrophobicity in the crystallization behavior of PLA. They observed a tendency of the more hydrophobic clays to hinder the re-arrangement of the PLA molecules into organized crystalline structures. Furthermore, they verified the PLA molecules in the composites with intermediate to extremely hydrophobic clays were less mobile. The PLA molecules in the amorphous phase of the composites with the least hydrophobic clays were much more mobile.

Therefore, according to the Table 3, the Cloisite 30B accelerates the isothermal crystallization of the PDLLA

in the composites and Cloisite 20A hinders it. This result is coherent with the previous results showed in this work.

3.4 Equilibrium melting point (Tm°)

The equilibrium melting point of a polymer (Tm^0) can be defined as the equilibrium between a set crystal with the melt polymer, wherein the effects of large size and the melt polymer surface are negligible. Actually, the polymers present small and imperfect crystals that melt at temperatures below Tm°. As the crystal morphology is influenced by the crystallization temperature, the experimentally observed melting temperature typically increases almost linearly with increasing crystallization temperature[15].

Theoretically, the equilibrium melting point may be deduced by plotting the observed apparent melting temperature (Tm) against the crystallization temperature (Tc)[31]. The equilibrium melting temperature can be extrapolated from the intersection of the resulting straight line to the line Tm = Tc and the dependence of Tm on Tc is given by Equation (6).

$$T_m = T_m^0 \left(1 - \frac{1}{2\beta}\right) + \frac{1}{2\beta} T_c \qquad (6)$$

where Tm^0 is the equilibrium melting point and β describes the growth of lamellar thickness during crystallization. Under equilibrium conditions, β equals 1.

The Hoffmann-Weeks plots of the DSC data and the values of Tm^0 are reported in Figure 6[27]. They are approximately

161 ºC for the three nanocomposites. These values are close to those found in the literature, between 120 and 180 ºC depending on the D-lactide content. Santis et al.[32] found a similar value at around 160ºC. Saeidlou[6] compares the melting point data from several authors as a function of D-unit content in the polymer structure. Pure PLLA (0% D-lactate) exhibits the maximum melting temperature, between 175 and 180 ºC. The melting point decreases linearly with the D-lactate content. Variations may be due to variations in molecular weights and the purity of the investigated polymers[6,8].

The obtained values for the PDLLA and the nanocomposites were very similar, which indicates that the organoclays do not affect the crystal structure, although a light reduction for the PDLLA30B could be associated to certain level of compatibility.

3.5 Ozawa theory

The non-isothermal crystallization of the PDLLA and the nanocomposites were investigated under different heating rates. From the Figure 2, it is notable that the values of $T_{cc\ onset}$ under different heating rates, are not equal, being a result of a rate-dependent induction time preceding the initiation of crystallization. As can be noted that $T_{cc\ onset}$ increases with the increase of the heating rate. This behavior occurs because in a lower heating rate, there is more time to overcome the nucleation barrier, so that the cold crystallization of the polymer starts at lower temperatures, while higher
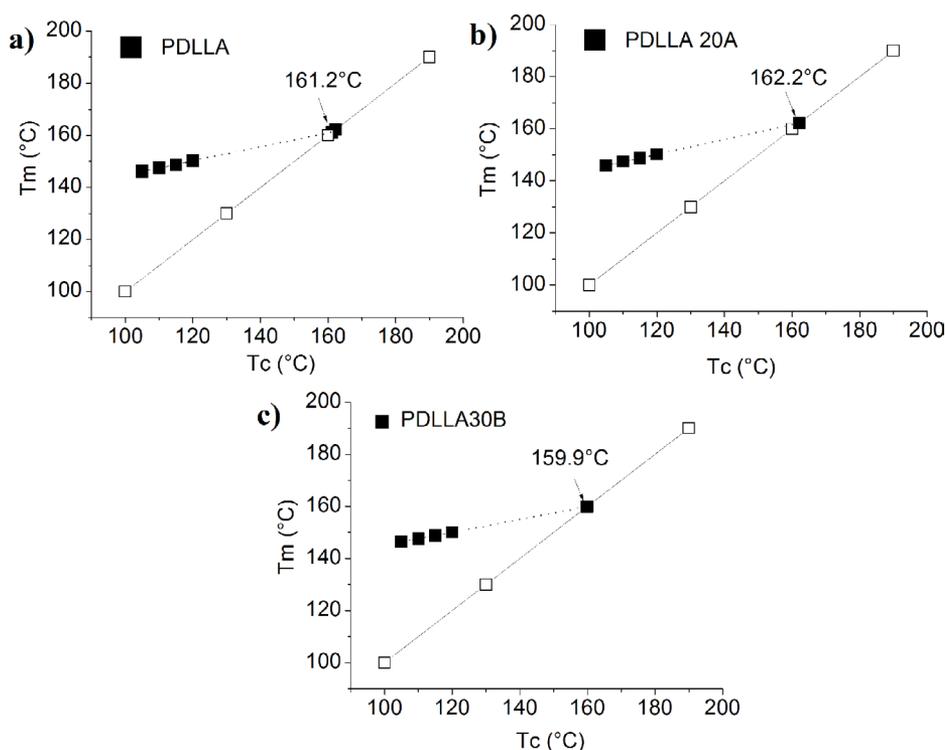

Figure 6. Melting point (Tm) as a function of the crystallization temperature (Tc). The extrapolation of the lines of the experimental data to Tm = Tc are shown as dashed lines; (a) PDLLA, (b) PDLLA20A, (c) PDLLA30B. Reproduced from Ref.[27], with permission of 13th Congresso Brasileiro de Polímeros - CBPol/Associação Brasileira de Polímeros - ABPol.

heating rate, nucleation starts at higher temperatures. The exothermal curves of heat flow as function of the temperature, for a heating rate of 1.5 ºC min^{-1} are illustrated in Figure 7. It is observed that the presence of Cloisite 30B promotes a decrease in T$_{cc\ onset}$ of PDLLA, and the opposite occurs to the PDLLA20A in accordance with the isothermal study.

Integration of the exothermal peaks during the nonisothermal scan can give the relative degree of crystallization (X(T)) as a function of temperature (T), shown in Figure 8. It is observed that the PDLLA and PDLLA30B samples submitted to lower heating rate crystallized at a lower temperature range and a longer time interval, thus the crystallization process is controlled by nucleation[33]. However, for the sample PDLLA20A the opposite occurs, this means that

the crystallization process is controlled by crystal growth or the nucleation is being hampered.

Ozawa modified the Avrami equation to account for the effect of cooling rate (φ) on nonisothermal crystallization. This method can be used when crystallization occurs at a constant cooling rate. According to Ozawa theory, the relative degree of crystallization at temperature T, X(T), can be calculated by the Equation (7).

$$X(T) = 1 - \exp\left(-\frac{K(T)}{\varnothing^m}\right) \qquad (7)$$

Where φ is the cooling rate, K(T) is the cooling function, which is related to the crystallization rate and indicates how fast crystallization proceeds, and m is the Ozawa exponent that depends on the dimension of crystal growth[34]. The Ozawa method was adapted to the cold crystallization of the PDLLA for different heating rates. By plotting ln[-ln(1-K(T))] vs. ln φ^{-1}, a straight line can be obtained as shown in Figure 9, and the kinetics parameters m and K(T) can be derived from the slope and the intercept, respectively. The results from Figure 10 for different temperatures are listed in Table 4.

The curves of Figure 9 show that initially the development of the crystallinity with temperature is slow to PDLLA20A, which means that Cloisite20A delayed nucleation rate of PDLLA. However, for the PDLLA30B the crystallization is faster and at lower temperatures, indicating a higher crystallization rate that can also be observed for the values of K in Table 4. The K value in low temperature, for example 100 ºC, for PDLLA30B is the highest one, which agrees with the previously stated.
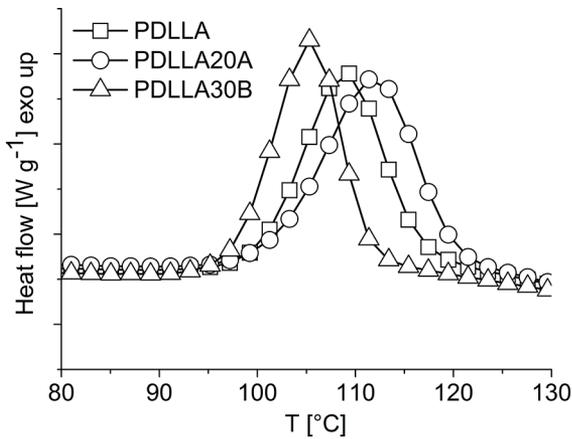

Figure 7. Cold crystallization curves for the PDLLA and the nanocomposites at 1.5°Cmin^{-1} heating rate (second heating).
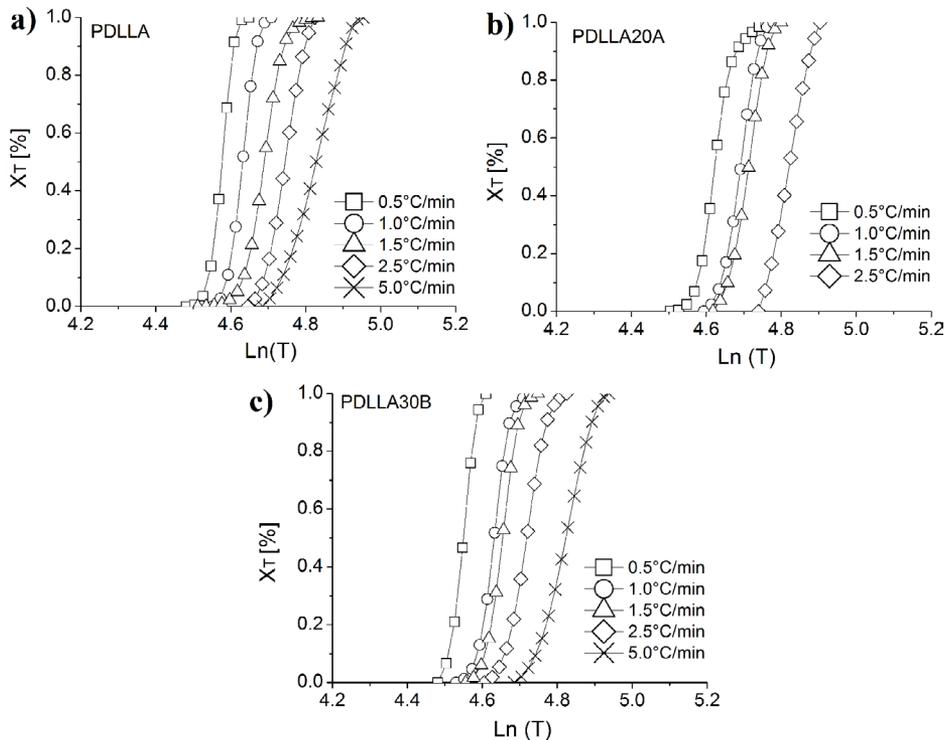

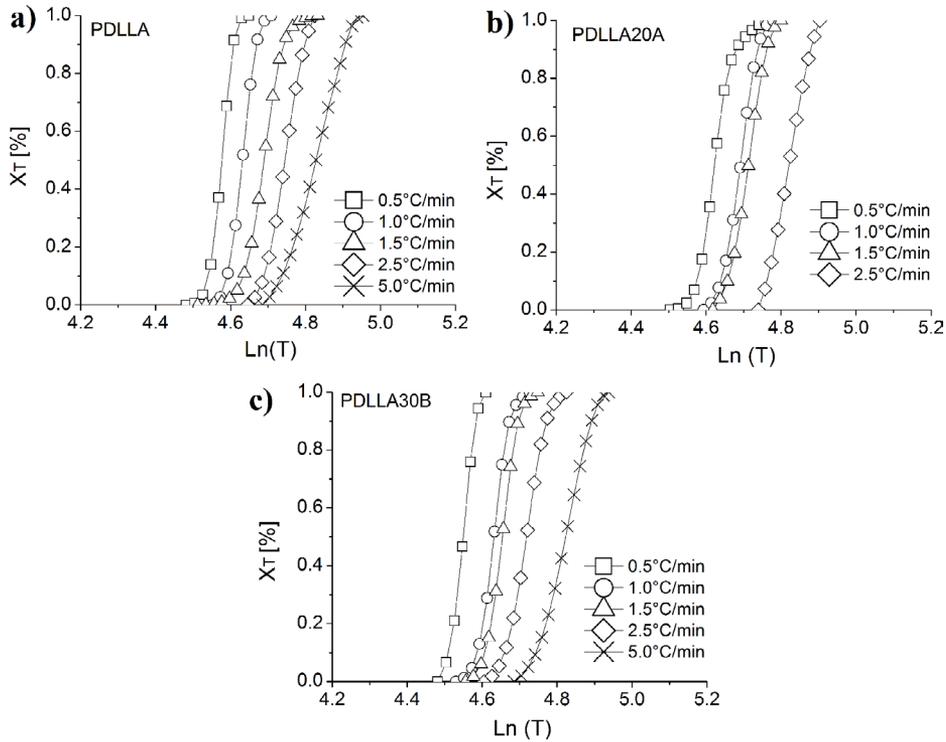**Figure 8.** Relative crystallinity versus crystallization temperature: (a) PDLLA, (b) PDLLA20A, (c) PDLLA30B.

Figure 9. Ozawa curves for non-isothermal cold crystallization: (a) PDLLA, (b) PDLLA20A, (c) PDLLA30B.

Table 4. Ozawa kinetics parameters as a function of crystallization temperature and Activation energy calculated according to the Kissinger method.

Samples	T		m	K(T) 10⁻³	DE$_a$
	°C			s⁻¹	(J.mol⁻¹)
PDLLA	96		3.6	35.8	
	98		3.6	103.3	
	100		3.4	249.1	116.4
	102		3.3	537.9	
PDLLA20A	102		2.9	103.3	
	104		2.4	239.3	
	106		2.1	444.9	123.5
	108		1.7	748.3	
	110		1.3	1161.8	
	112		1.0	1733.3	
PDLLA30B	96		4.1	71.4	
	98		3.6	208.0	113.8
	100		3.5	522.0	

The Ozawa exponent varies with temperature, as noted in Table 4, thereby in low temperature the samples show m values between 3 and 4, in accordance with observed by Avrami theory.

3.6 Activation energy

The equation for determining the activation energy of the nonisothermal crystallization developed by Kissinger

considers the influence of the various heating/cooling rates employed during the crystallization process[32]. Kissinger reported that the activation energy can be determined according to Equation (8).

$$\ln\left(\frac{\varnothing}{T_c^2}\right) = -\frac{\Delta E_a}{R} \cdot \frac{1}{T_c} \tag{8}$$

where R is the gas constant and Tc is the crystallization temperature in Kelvin.

The crystallization activation energy (ΔE_a) is determined by the slopes of the plots of $\ln(\varphi/T_c^2)$ versus $1/T_c$ by Kissinger Equation (8).In the current study, the ΔE_a values for PDLLA and the nanocomposites are listed in Table 4. In agreement with results of isothermal and nonisothermal crystallization, the activation energy was lower for the PDLLA30B nanocomposite than for the PDLLA and it was higher for the PDLLA20A.

Xu et al.[35] have studied the isothermal crystallization of intercalated and exfoliated polyethylene/montmorillonite nanocomposites. They found larger crystallization activation energy of the intercalated sample, originates from its higher transport activation energy, which they attributed to the PE chains to be confined between the clay layers and to have poor mobility.

3.7 Rheological properties

The nanocomposites dynamic rheological behavior was studied. The G'and G" versus ω are shown in Figure 10. The terminal zone is the curve portion which gives the information
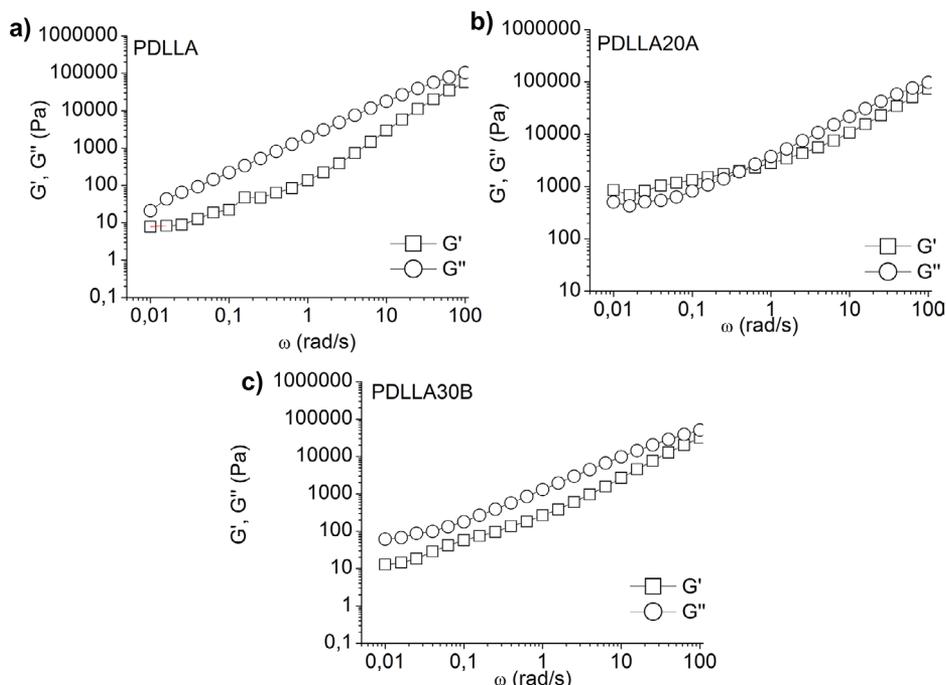
Figure 10. G' and G" versus frequency at 180°C: (a) PDLLA, (b) PDLLA20A, (c) PDLLA30B.

regarding to the rheological behavior change. The Table 5 presents the slope of G' versus ω of the terminal zone (a). The PDLLA presented α of 2.10 while PDLLA20A and PDLLA30B presented α of 0.33 and 0.78 respectively. For polymer melts, typically α is 2, G' ~ ω^2 and G" > G', while for solid polymers, this slope tends to zero, G' ~ ω^0) and G' > G"[36]. The PDLLA30B had a small slope value but G" > G', while the PDLLA20A had G' > G" at low frequencies and a very close to zero indicating that this sample presented a pseudosolid behavior associated to a percolated network[37].

The complex viscosity versus ω curve for the nanocomposites are shown in Figure 11. It was observed that the rheological behavior of PDLLA is completely modified by the presence of clays. The PDLLA showed a wide Newtonian plateau between 0.01 and 10 rad/s. The addition of clay made this plateau to disappear completely, especially for PDLLA20A sample, and the nanocomposite starts to get a pseudoplastic behavior.

Furthermore, it was observed that the PDLLA30B showed a smaller viscosity than the PDLLA at high frequencies. This typically happens when there is a degradation of polymer. In order to understand this result, was seen in the study carried out by Souza et al.[14] the molecular weight for the same samples studied here. They found that there was a decrease in molecular weight after incorporation of the clays, which was more pronounced for the sample containing Cloisite 30B, which showed a reduction of 44% in M_w. These results suggest that the introduction of this clay causes degradation of PDLLA greater than for the pure polymer during processing. So, the polymer degradation is one of the

factors that may be influencing the crystallization kinetics of this nanocomposite.

3.8 Isothermal Flow-Induced Crystallization

Normally, the crystallization process is different when the samples are analyzed in a quiescent method and under shear. So, with the flow-induced method, it is possible to understand the influence of the clays in the crystallization mechanism of the PDLLA under deformation. Figure 12 shows the shear stress versus time curve after application of a shear rate.

The flow induced crystallization behavior of the three samples is similar to that observed by Farah and Bretas[19] that was described as: at short time, the τ was very low and constant; when τ begun to increase this indicated that the nucleation took place as the first step of the crystallization. At this point the induction crystallization time (t_i) was measured; suddenly the τ decreased due to the heat released during the crystallization causing the material viscosity to decrease; and at the final step of the crystallization process, at high times, the τ increases abruptly due to crystal growth. At this point the time for crystals growth (t_{growth}) was measured. The results are shown in Table 5.

The nanocomposites showed the lowest time for the nucleation and crystals growth. These results are the opposite observed in the DSC analysis. In the case of crystallization under deformation, the crystals are aligned along the flow and the chain orientation of the PDLLA macromolecules was further increased. Therefore, the flow-induced crystallization was faster for the nanocomposites than for PDLLA.

Table 5. Reological properties, Induction crystallization time and Structural recovery parameters for PDLLA and its nanocomposites

Sample	Rheological properties	Inductioncrystallization time		Structural recoveryparameters	
	a G'(w)	$t_i(s)$	$t_{growth}(s)$	$G'_{equi}(Pa)$	$t_{equi}(min)$
PDLLA	2.10	61	985	24	-
PDLLA20A	0.33	19	693	474	22.2
PDLLA30B	0.78	19	748	189	7.35
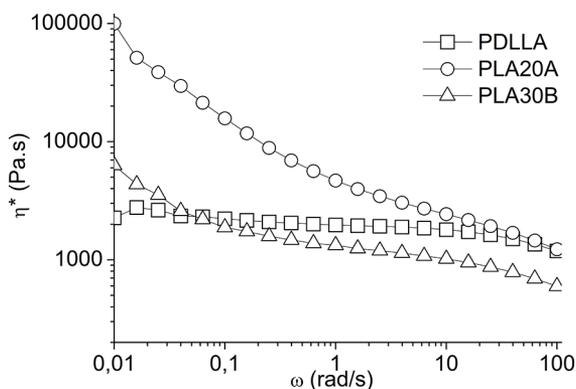
Figure 11. η^* versus frequency at 180°C for the PDLLA, PDLLA20A and PDLLA30B.
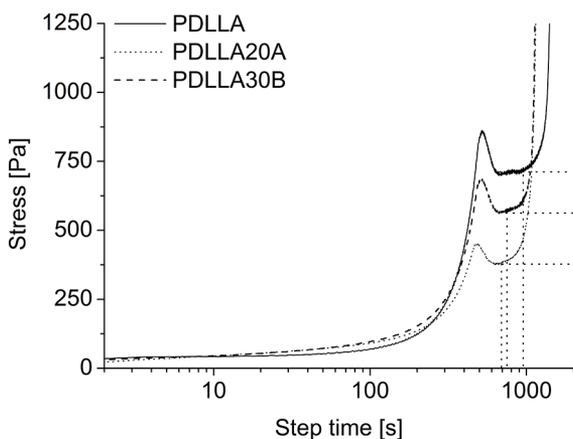
Figure 12. Shear stress (τ) versus time for the PDLLA, PDLLA20A and PDLLA30B.

3.9 Structural Recovery

In order to understand the mechanism, which governs the retardation of the PDLLA crystallization with the incorporation of clay Cloisite 20A, a method described by Wang et al.[20] was used. This method aims to study the confinement mechanism of PDLLA chains in PDLLA20A sample associated with the three-dimensional network formed by the clay sheets.

As described, a steady shear deformation was applied to the molten polymer, and the chains and clay sheets were aligned parallel to the direction of the shear stress, Figure 13 (b). The initial connections, including the entanglement between the molecular chains and electrostatic attraction of tactoids/clay sheets are disrupted and destroyed during the deformation process. After deforming the materials, the G' was monitored as a function of time to determine the time required for the structural recovery (t_{equi}). The curves are represented in the Figure 14. The Table 5 shows the t_{equi} and G'(equi).

It is observed that the PDLLA showed no variation of G' over time, which means that the recovery is very fast. The PDLLA30B sample exhibited a t_{equi} about 7 minutes, while the PDLLA20A showed the longest time, about 22 minutes.

The magninute of t_{equi} can represent the kinetics of structural recovery and relaxation[20]. Therefore, the PDLLA20A sample has greater restriction to mobility, that could be explained by been due to geometric confinement in a three-dimensional network formed with the clay sheets.

4. Conclusions

Isothermal and nonisothermal crystallization kinetics of the PDLLA were studied with organically modified clay to explore the effect of polarity of different clay's organic modifiers in the crystallization process of the PDLLA and its correlation with the rheological properties. Two different commercially available organoclays were used, Cloisite 20A e Cloisite 30B. The clay altered the crystallization behavior of PDLLA but in different unexpected manner. The Cloisite 30B, clay modified with a hydrophilic surfactant, acts as a nucleating agent what is attributed to the high compatibility and to the polymer degradation, which contributed to an increase of the crystallinity and crystallization rate. In the case of Cloisite 20A, clay modified with a hydrophobic surfactant, there is a retardation of nucleation and a lower crystallinity degree, possibly due to inhibition of mobility of the polymer chains, caused by the geometric confinement in a three-dimensional network formed with the clay sheets. The Avrami and Ozawa exponents showed a three-dimensional spherulitic growth for all samples and the obtained equilibrium melting point for the PDLLA was 161°C, been slightly altered as function of the surfactant polarity in the clay.
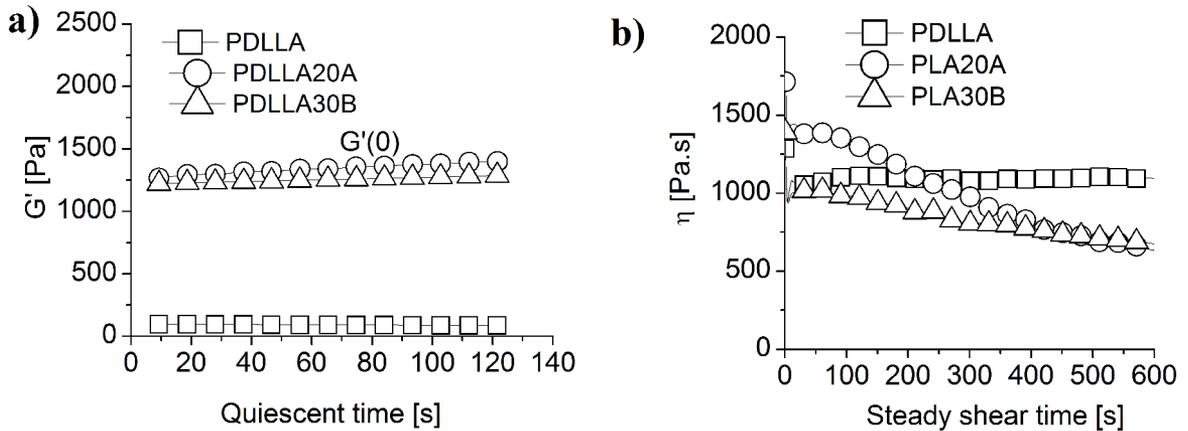
5. Acknowledgments

Figure 13. Structural recovery experiments: initial G' measured under deformation (a) and viscosity monitored under a constant deformation (b).
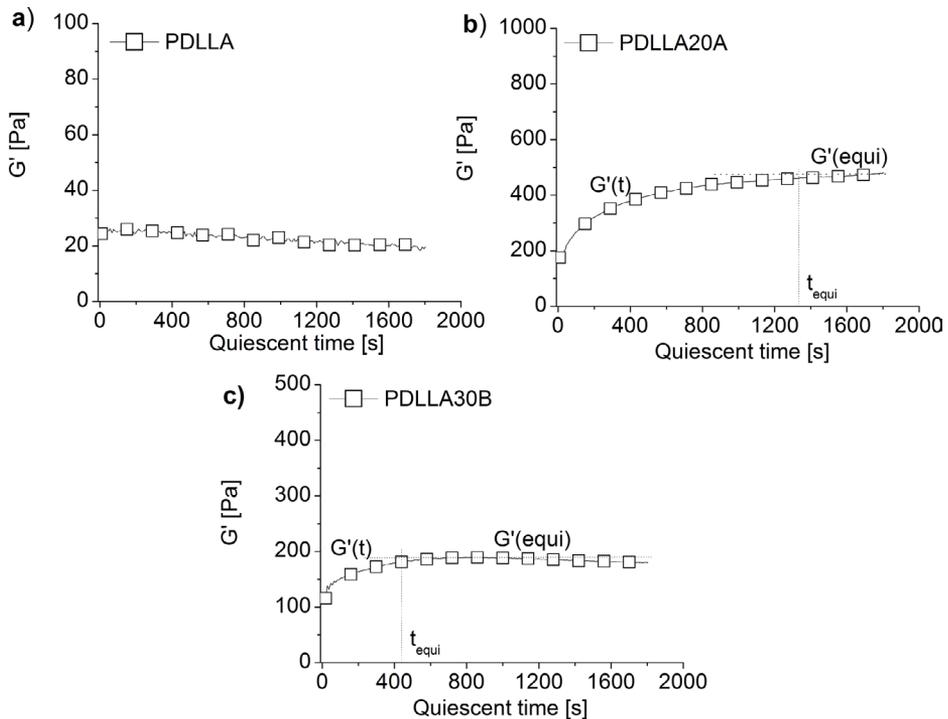

Figure 14. G' versus time curve measured after deformation. Structural recovery tests: (a) PDLLA, (b) PDLLA20A, (c) PDLLA30B.

6. References

1. Tsuji H, Takai H, Fokuda N, Takikawa H. Non-Isothermal Crystallization Behavior of Poly(L-lactic acid) in the Presence of Various Additives. *Macromolecular Materials and Engineering*. 2006;291(4):325-335.

2. Cai M, Liu L, Wang L, Yao K, Li S, Xiong H. Isothermal crystallization kinetics of thermoplastic starch/poly(lactic acid) composites. *Carbohydrate Polymers*. 2011;86(2):941-947.

3. Souza PMS, Morales AR, Marin-Morales MA, Mei LHI. PLA and Montmorilonite Nanocomposites: Properties, Biodegradation and Potential Toxicity. *Journal of Polymers and the Environment*. 2013;21(3):738-759.

4. Nam JY, Ray SS, Okamoto M. Crystallization Behavior and Morphology of Biodegradable Polylactide/Layered Silicate Nanocomposite. *Macromolecules*. 2003;36(19):7126-7131.

5. Nam JY, Okamoto M, Okamoto H, Nakano M, Usuki A, Matsuda M. Morphology and crystallization kinetics in a mixture of low-molecular weight aliphatic amide and polylactide. *Polymer*. 2006;47(4):1340-1347.

6. Saeidlou S, Huneault MA, Li H, Park CB. Poly(lactic acid) crystallization. *Progress in Polymer Science*. 2012;37(12):1657-1677.

7. Iannace S, Nicolais L. Isothermal crystallization and chain mobility of poly(L-lactide). *Journal of Applied Polymer Science*. 1997;64(5):911-919.

8.   Krikorian V, Pochan DJ. Unusual Crystallization Behavior of Organoclay Reinforced Poly(l-lactic acid) Nanocomposites. *Macromolecules*. 2004;37(17):6480-6491.

9.   Krikorian V, Pochan DJ. Crystallization Behavior of Poly(l-lactic acid) Nanocomposites:? Nucleation and Growth Probed by Infrared Spectroscopy. *Macromolecules*. 2005;38(15):6520-6527.

10.   Liao R, Yang B, Yu W, Zhou C. Isothermal cold crystallization kinetics of polylactide/nucleating agents. *Journal of Applied Polymer Science*. 2007;104(1):310-317.

11.   Li Y, Wu A, Wang Y, Liu L, Han L, Wu J, et al. Synergistic effects of PEG and MWCNTs on crystallization behavior of PLLA. *Journal of Applied Polymer Science*. Part B: Polymer Physics. 2010;48(5):520-528.

12.   Li HB, Huneault MA. Effect of nucleation and plasticization on the crystallization of poly(lactic acid). *Polymer*. 2007;48(23):6855-6866.

13.   Fukushima K, Tabuani D, Camino G. Nanocomposites of PLA and PCL based on montmorillonite and sepiolite. *Materials Science and Engineering: C*. 2009;29(4):1433-1441.

14.   Souza PMS, Corroqué NA, Morales AR, Marin-Morales MA, Mei LHI. PLA and Organoclays Nanocomposites: Degradation Process and Evaluation of ecotoxicity Using Allium cepa as Test Organism. *Journal of Polymer and the Environment*. 2013;21(4):1052-1063.

15.   Wokadala OC, Ray SS, Bandyopadhyay J, Wesley-Smith J, Emmambux NM. Morphology, thermal properties and crystallization kinetics of ternary blends of the polylactide and starch biopolymers and nanoclay: The role of nanoclay hydrophobicity. *Polymer*. 2015;71:82-92.

16.   Cloisite® Technical Data Sheets. Available from: <http://www.matweb.com/search/GetMatlsByTradename.aspx?tn=Cloisite%C2%AE>. Access in: 14/09/2018.

17.   Souza PMS, Morales AR, Mei LHI, Marin-Morales MA. Estudo da influência de argilas organofílicas no processo de biodegradação do PLA. *Polímeros*. 2014;24(1):110-116.

18.   Yasuniwa M, Tsubakihara S, Sugimoto Y, Nakafuku C. Thermal analysis of the double-melting behavior of poly(L-lactic acid). Journal of Applied Polymer Science. *Part B: Polymer Physics*. 2004;42(1):25-32.

19.   Farah M, Bretas RES. Characterization of i-PP shear-induced crystallization layers developed in a slit die. *Journal of Applied Polymer Science*. 2004;91(6):3528-3541.

20.   Wang K, Liang S, Deng J, Yang H, Zhang Q, Fu Q, et al. The role of clay network on macromolecular chain mobility and relaxation in isotactic polypropylene/organoclay nanocomposites. *Polymer*. 2006;47(20):7131-7144.

21.   Fukushima K, Fina A, Geobaldo F, Venturello A, Camino G. Properties of poly(lactic acid) nanocomposites based on montmorillonite, sepiolite and zirconium phosphonate. *eXPRESS Polymer Letters*. 2012;6(11):914-926.

22.   Fukushima K, Abbate C, Tabuani D, Gennari M, Camino G. Biodegradation of poly(lactic acid) and its nanocomposites. *Polymer Degradation and Stability*. 2009;94(10):1646-1655.

23.   Pereira RB, Morales AR. Estudo do comportamento térmico e mecânico do PLA modificado com aditivo nucleante e modificador de impacto. *Polímeros*. 2014;24(2):198-202.

24.   Fambri L, Migliaresi C. Crystallization and Thermal Properties. In: Auras R, Lim LT, Selke SEM, Tsuji H, eds. *Poly(Lactic Acid): Synthesis, Structures, Properties, Processing, and Applications*. Hoboken: John Wiley & Sons; 2010. p. 114-118.

25.   Kawai T, Rahman N, Matsuba G, Nishida K, Kanaya T, Nakano M, et al. Crystallization and Melting Behavior of Poly (l-lactic Acid). *Macromolecules*. 2007;40(26):9463-9469.

26.   Zhang J, Tashiro K, Tsuji H, Domb AJ. Disorder-to-Order Phase Transition and Multiple Melting Behavior of Poly(l-lactide) Investigated by Simultaneous Measurements of WAXD and DSC. *Macromolecules*. 2008;41(4):1352-1357.

27.   Ramos RBB, Souza PMS, Morales AR (2015). Cinética de cristalização isotérmica e temperatura de fusão de equilíbrio de nanocompósitos de PDLA. In: *13th Congresso Brasileiro de Polímeros*. Natal, RN: ABPol.

28.   Xu J, Shi W. Synthesis and crystallization kinetics of silsesquioxane-based hybrid star poly(e-caprolactone). *Polymer*. 2006;47(14):5161-5173.

29.   Lorenzo AT, Arnal ML, Albuerne J, Müller AJ. DSC isothermal polymer crystallization kinetics measurements and the use of the Avrami equation to fit the data: Guidelines to avoid common problems. *Polymer Testing*. 2007;26(2):222-231.

30.   Di Lorenzo ML, Silvestre C. Non-isothermal crystallization of polymers. *Progress in Polymer Science*. 1999,24(6):917-950.

31.   Wunderlich B. *Macromolecular Physics, Volume 2, Crystal Nucleation, Growth, Annealing*. New York: Academic Press; 1976.

32.   Hoffman JD, Weeks JJ. Melting Process and the Equilibrium Melting Temperature of Polychlorotrifluoroethylene. *Journal of Research of the National Bureau of Standards, Section A: Physics and Chemistry*. 1962;66A(1):13-28.

33.   De Santis F, Pantani R, Titomanlio G. Nucleation and crystallization kinetics of poly(lactic acid). *Thermochimica Acta*. 2011;522(1-2):128-134.

34.   Gonella LB. *Nanocompósito de poliamida 6 com MMT e xisto*. [Thesis]. Porto Alegre: Federal University of Rio Grande do Sul; 2007.

35.   Li J, Zhou C, Wang G, Tao Y, Liu Q, Li Y. Isothermal and nonisothermal crystallization kinetics of elastomeric polypropylene. *Polymer Testing*. 2002;21(5):583-589.

36.   Xu JT, Zhao YQ, Wang Q, Fan ZQ. Isothermal crystallization of intercalated and exfoliated polyethylene/montmorillonite nanocomposites prepared by in situ polymerization. *Polymer*. 2005;46(25):11978-11985.

37.   Favaro MM, Branciforti MC, Bretas RES. Influence of a terpolymer compatibilizer on the nanostructure of poly(trimethylene terephthalate)/montmorillonite nanocomposites. *Polymers for Advanced Technologies*. 2009;20(12):940-949.